NRC Research Press

ARTICLE

p- and n-type microcrystalline silicon oxide (μc-SiO_x:H) for applications in thin film silicon tandem solar cells[1]

V. Smirnov, A. Lambertz, S. Tillmanns, and F. Finger

Abstract: We report on the development and application of p- and n-type hydrogenated microcrystalline silicon oxide (μc-SiO_x:H) alloys in tandem thin film silicon solar cells. Our results show that the optical, electrical, and structural properties of μc-SiO_x:H can be conveniently tuned over a wide range to fulfil the requirements for solar cell applications. We have shown that adding of PH_3 gas during deposition tends to increase crystallinity of μc-SiO_x:H layers, while additional trimethylboron (TMB) tends to suppress crystalline growth. When applied in tandem solar cells, both p- and n-type μc-SiO_x:H lead to a remarkable increase in the top cell current. Taking advantage of low refractive index and high optical band gap of μc-SiO_x:H allows the achievement of high efficiencies of 13.1% (initial) and 11.8% (stabilized).

PACS Nos.: 88.40.hj, 88.40.jj, 78.66.Jg.

Résumé : Nous discutons du développement et de l'utilisation d'alliages d'oxyde de silicium microcristallin (μc-SiO_x:H) hydrogéné de types p et n, en tandem avec des films minces de silicium comme cellules solaires. Nos résultats montrent que les propriétés optiques, électriques et structurales du μc-SiO_x:H peuvent être ajustées sur un large domaine, afin de remplir les exigences d'applications en tant que cellules solaires. Nous montrons que l'ajout de PH_3 pendant l'opération de dépôt augmente la cristallinité des couches de μc-SiO_x:H, alors que l'ajout de TMB la diminue. Lorsque utilisés en tandem comme cellules solaires, les deux types, p et n de μc-SiO_x:H mènent à une augmentation remarquable du courant. Prenant avantage d'un faible indice de réfraction et d'une large bande interdite optique, nous atteignons des rendements (initial) de 13.1 % et de 11.8 % (stabilisé). [Traduit par la Rédaction]

1. Introduction

As a wide optical gap material, microcrystalline silicon oxide (μc-SiO_x:H) has been the subject of research as a material for photovoltaic applications [1–10]. μc-SiO_x:H, being a two phase material, is a mixture of microcrystalline silicon (μc-Si:H) and amorphous silicon oxide (a-SiO_x:H) [5, 6]. The properties of μc-SiO_x:H thin films are influenced by the doping, crystalline fraction, and the oxygen content. Optical band gap (E_{04}), refractive index (n), crystallinity (I_{CRS}), and conductivity can be modified over a wide range by varying gas flows during material growth.

Here we present the development and application of p- and n-type μc-SiO_x:H alloys, prepared over a wide range of compositions, for application in tandem junction thin film silicon solar cells. We show that p-type as well as n-type μc-SiO_x:H alloys with enhanced optical band gap energy, low refractive index, and suitable electrical properties are beneficial for usage in tandem solar cells. In the case of tandem devices, the n/p contact between amorphous silicon (a-Si:H) and μc-Si:H component cells can be substituted by μc-SiO_x:H doped layers [2, 5–10] to enable reflection of short wavelength light back to the top (a-Si:H) cell because of a step in refractive index. This enhances the top cell current without an increase in the thickness of the a-Si:H absorber layer. Additionally the n-type μc-SiO_x:H can be applied as an n-layer of the μc-Si:H bottom cell leading to reduced parasitic absorption. With the aid of μc-SiO_x:H doped layers, high efficiencies of 13.1% (initial) and 11.8% (stabilized) were achieved in the present work, for tandem solar cells.

2. Experimental

p- and n-type μc-SiO_x:H layers were deposited using the radio frequency (13.56 MHz) plasma enhanced chemical vapour deposition technique at 185 °C substrate temperature and a power of 50 W, using a mixture of silane (SiH_4), hydrogen (H_2), and carbon dioxide (CO_2) gases. Trimethylboron (TMB) phosphine (PH_3) gases were used for p- and n-type doping, respectively. The layers were deposited at varied CO_2 flow ratio r_{CO2} defined as the ratio between the CO_2 flow and the SiH_4 flow. Additional details on the deposition conditions can be found elsewhere [7–10]. Optical and electrical properties of these layers were investigated by photothermal deflection spectroscopy and conductivity measurements, respectively. Conductivity measurements were performed on films equipped with coplanar electrodes 5 mm in lengths separated by a 0.5 mm gap. The structural properties of μc-SiO_x:H layers were probed using Raman spectroscopy. The ratio of integrated intensities attributed to crystalline and amorphous regions, $I_{CRS} = I_c/(I_c + I_a)$ was used as semiquantitative value of the crystalline volume fraction [11].

μc-SiO_x:H layers were subsequently used as an intermediate reflector and as an n-layer of the μc-Si:H bottom cell in tandem solar cells. Silicon thin films were deposited using the plasma enhanced chemical vapour deposition technique using either radio frequency (p-, i-, n-layers of the top cell, and n-layer of the bottom cell) or very high frequncy (94.7 MHz, p- and i-layers of the bottom cell) excitation. Solar cells were deposited on SnO_2:F coated glass substrates from the Asahi Glass Company (type VU). Additional details on the preparation of the solar cells can be found in refs. 9 and 11. Solar cells were characterised by current–

Received 25 October 2013. Accepted 11 February 2014.

V. Smirnov, A. Lambertz, S. Tillmanns, and F. Finger. IEK-5 Photovoltaik, Forschungszentrum Jülich GmbH, D-52425 Jülich, Germany.
Corresponding author: V. Smirnov (e-mail: v.smirnov@fz-juelich.de).

[1]This paper was presented at the 25th International Conference on Amorphous and Nanocrystalline Semiconductors (ICANS25).

Fig. 1. Crystallinity (I_{CRS}) of μc-SiO_x:H films prepared at varied (*a*) PH_3 flow, and (*b*) TMB flow, presented as a function of r_{CO2}.

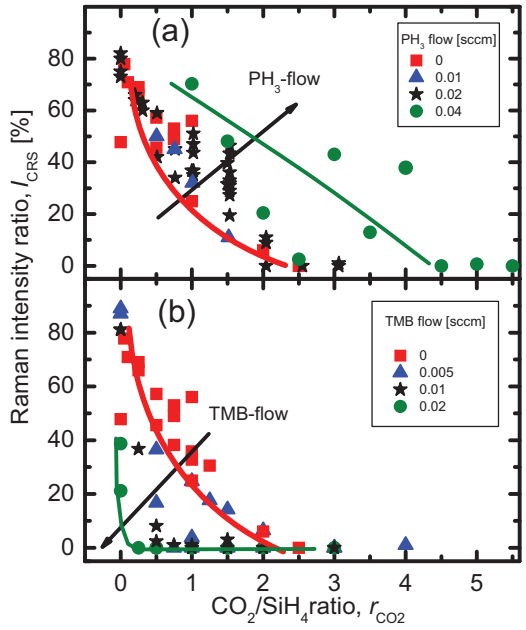

voltage (*J*–*V*) measurements under AM 1.5 illumination using a double source (Class A) sun simulator, and by quantum efficiency (QE) measurements, additional details are given in ref. 9. The light soaking of the solar cells was performed at 55 °C in the open circuit condition, using metal halide lamps with an intensity of 1000 W/m² in the sample plane and a class B spectrum [12].

3. Results

3.1. Material properties

Figure 1 presents the crystallinity (I_{CRS}) of μc-SiO_x:H films, as a function of r_{CO2}, depending on the PH_3 (Fig. 1*a*) and TMB (Fig. 1*b*) flows. It is seen that I_{CRS} decreases with increasing r_{CO2} for all of the series of dopant gas flows. In the case of n-type μc-SiO_x:H films, an increase in PH_3 flow results in an increase in (I_{CRS}) at a given r_{CO2}. For example, in the case of the layers prepared at high r_{CO2} of 1, (I_{CRS}) increases from around 25% up to around 70% with increasing PH_3 flow from 0 up to 0.04 sccm. In contrast, an increase in TMB flow (Fig. 1*b*) results in the reduction of crystallinity at a given r_{CO2} ratio.

The corresponding dark conductivity values are presented in Fig. 2 versus the optical band gap (E_{04}). Such presentation serves as a figure of merit for the suitability for the materials for applications in tandem solar cells. For both n- and p-type μc-SiO_x:H films (Fig. 2*a* and 2*b*, respectively) the general trend indicates a reduction in dark conductivity with increasing optical band gap (E_{04}): σ_{dark} reduces from around 10 S/cm down to below 10^{-12} S/cm with increasing E_{04} from 1.9 to 2.9 eV (2.6 eV) in the case of n-type (p-type) μc-SiO_x:H films.

3.2. Tandem a-Si:H/μc-Si:H solar cells

A schematic structure of the a-Si:H/μc-Si:H tandem solar cells with integrated p- and n-type doped μc-SiO_x:H material is shown in Fig. 3. Selected n- and p-type μc-SiO_x:H layers were subsequently used as an intermediate reflector between a-Si:H and μc-Si:H component cells and additionally as an n-type contact layer (n2) in μc-Si:H bottom cell. The properties of these layers are listed in Table 1.

The resulting current densities calculated from the external QEs of the a-Si:H top cell ($J_{QE,Top}$) and of the μc-Si:H bottom cell ($J_{QE,Bot}$) and also the sum of both cells ($J_{QE,Sum}$) are shown in Fig. 4 for various cell structures, where the legend on the *x*-axis denotes the parts of the tandem solar cell where the μc-SiO_x:H was utilized.

Figure 4 shows in the case of the standard tandem cell, where no μc-SiO_x:H layer is used ("no SiO_x", cell 1), the current densities of the top and bottom cells ($J_{QE,Top}$ and $J_{QE,Bot}$) are 13 and 14.2 mA/cm², respectively. For this cell the current matching requirements are not fulfilled because $J_{QE,Top}$ is 1.2 mA/cm² lower. The next solar cell, which has "μc-SiO_x:H as n1" (cell 2) with a refractive index of 2.3 as

Fig. 2. Dark conductivity (σ_{dark}) and optical band gap (E_{04}) of (*a*) n-type and (*b*) p-type μc-SiO_x:H layers. The changes in refractive index (*n*) indicated by arrows at the top. Dashed areas indicate the region of $\sigma_{dark} > 10^{-5}$ S/cm.

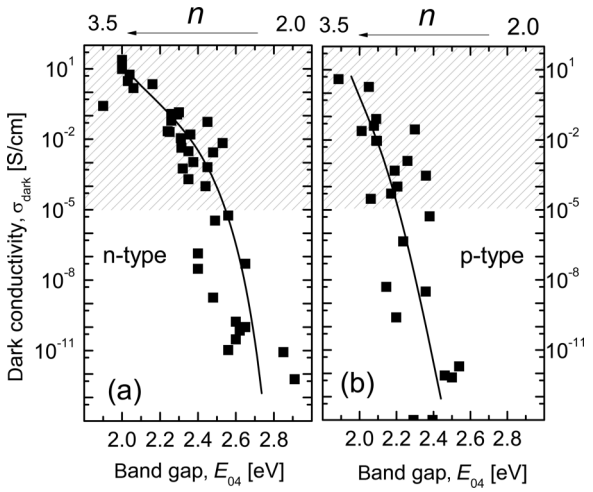

Fig. 3. Schematic diagram of a tandem solar cell. n1, p2, and n2 refer to n-layer of top cell, p-layer of bottom cell, and n-layer of bottom cell, respectively. The thickness of individual doped layers is around 25 ± 5 nm. The layers n1 and p2 form the n/p junction and act as an intermediate layer with a thickness of 50 ± 10 nm. The thicknesses of the intrinsic layers are around 400 and 3200 nm in the case of top and bottom cells, respectively.

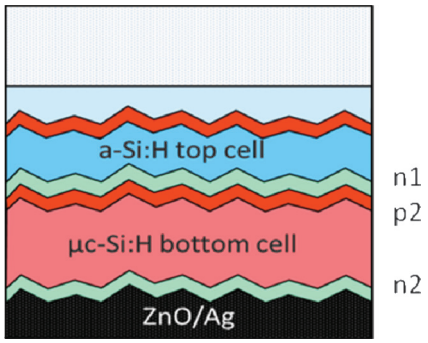

Table 1. Properties of μc-SiO_x:H layers used in tandem solar cells: dark conductivity (σ_{dark}), optical bandgap (E_{04}), and refractive index (*n*).

Layer	σ_{dark} (S/cm)	E_{04} (eV)	*n*
n1	10^{-3}	2.25–2.30	2.3–2.4
p2	10^{-3}	2.25	2.5
n2	10^{-2}	2.25	2.5

Fig. 4. Current densities calculated from the quantum efficiency for (squares) top cells, $J_{QE,Top}$; (circles) bottom cells, $J_{QE,Bot}$; and (triangles) sum, $J_{QE,Sum}$, for various cell structures. The application of the doped μc-SiO$_x$:H layers is described along the *x*-axis of the graph, corresponding to the solar cell numbers from 1 to 5 as indicated on the top.

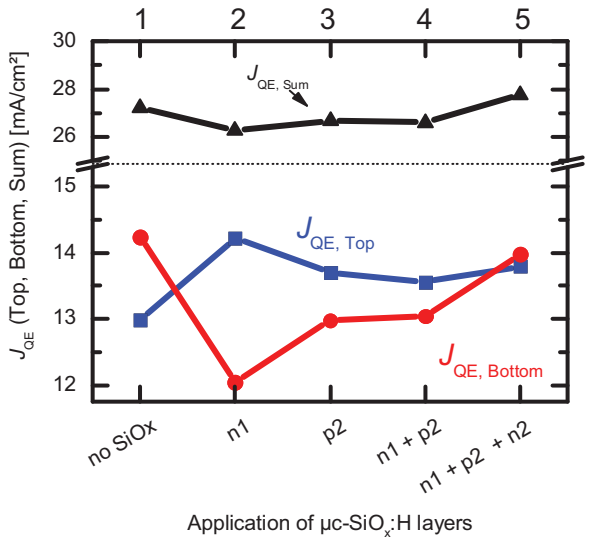

Fig. 5. QE and (1 – *R*) curves for tandem solar cells (solid line) with and (dashed line) without μc-SiO$_x$:H layers. The numbers show the gain in the current densities of top cells $J_{QE,Top}$ and total current $J_{QE,Sum}$ because of μc-SiO$_x$:H layers.

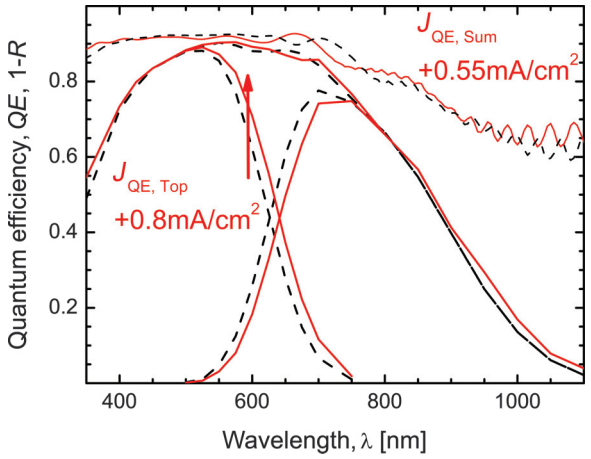

the intermediate reflector, $J_{QE,Top}$ is increased to 14.2 mA/cm² and $J_{QE,Bot}$ decreased to 12.1 mA/cm².

In a tandem solar cell with a p-type intermediate reflector (marked as "p2" in Fig. 4), the $J_{QE,Top}$ decreases to 13.7 mA/cm² and the $J_{QE,Bot}$ increases to 13 mA/cm² with respect to the previously mentioned cell. In the next solar cell (cell 4), n- and p-type μc-SiO$_x$:H are combined as an intermediate reflector in the n/p tunnel recombination junction (n1 + p2) of the tandem cell. Cell 5 has an additional μc-SiO$_x$:H layer as the n-layer of the bottom cell (n2) demonstrating a significant improvement in the $J_{QE,Bot}$ and $J_{QE,Sum}$. The QE curves of this solar cell are compared with a reference tandem solar cell (without μc-SiO$_x$:H) in Fig. 5. It can be seen that in the case of the solar cell with μc-SiO$_x$:H layers, QE of the top cell is enhanced in the wavelength region between 500 and 750 nm and QE of the bottom cell is enhanced in the wavelength region above 900 nm.

4. Discussion

The link between dark conductivity (σ_{dark}), crystallinity (I_{CRS}), and optical gap (E_{04}) is evident from Figs. 1 and 2. The results indicate that when r_{CO2} increases, I_{CRS} decreases while E_{04} increases, leading to a reduction of σ_{dark}, in agreement with previous reports [7–9]. In the case of p-type μc-SiO$_x$:H films, a strong reduction in I_{CRS} with increasing TMB flow is observed (Fig. 1*a*), indicating that the microcrystalline growth is suppressed by boron incorporation. Such behaviour is also known for the p-type μc-Si:H [13]. In contrast, in the case of phosphorous doping, an improvement of crystallinity at a given r_{CO2} is observed. An increase of the μc-Si:H fraction with increasing the phosphine flow can also be found in the literature [14] for μc-Si:H.

For the applications of doped μc-SiO$_x$:H in thin film solar cells, a sufficient dark conductivity above 10^{-5} S/cm is required [9] as indicated by the dashed area in Fig. 3. The trade-off between electrical and optical properties is also evident in Fig. 3. While the material with high E_{04} would be optically favourable to be used as doped layers in solar cells because of reduced parasitic absorption, the electrical properties of such μc-SiO$_x$:H layers are rather poor. That is why the layers with intermediate values of E_{04} (see Table 1) were selected for incorporation in tandem solar cells.

The favourable effect of the optical properties of μc-SiO$_x$:H is evident in Fig. 4. It is seen that both p- and n-type μc-SiO$_x$:H, when used as an intermediate reflector between the subcells, result in an increase in the top cell current. This can be related to a low refractive index, *n*, of μc-SiO$_x$:H (see Table 1), enhancing the reflection of short wavelength light into the top cell [2–5]. This is also accompanied by a reduction in $J_{QE,Bot}$ of the bottom cells, indicating a so-called "current transfer" from bottom to top component cells (enhanced absorption of light in the top cell and corresponding reduced absorption of light in the bottom cell, resulting in an increase in $J_{QE,Top}$ and a corresponding reduction in $J_{QE,Bot}$). The lower $J_{QE,Top}$ of cell 3 (where a p-type μc-SiO$_x$:H layer is used) with respect to a solar cell 2 (where an n-type μc-SiO$_x$:H layer is employed) is most likely related to the slightly higher refractive index, *n*, of 2.5 (see Table 1). In turn, an increase in $J_{QE,Bot}$ of cell 3 can be attributed to the reduced parasitic absorption, visible in the cell reflection curves as discussed in ref. 9. In the case of cell 4, $J_{QE,Bot}$ is slightly increased relative to cell 3, while $J_{QE,Sum}$ of cells 3 and 4 remain at a similar level because of slightly reduced top cell current $J_{QE\ top}$ of cell 4. The $J_{QE,Bot}$ of the bottom cell can be improved when an n2 μc-SiO$_x$:H layer is used instead of a standard a-Si:H n-layer. In the case of the tandem cell 5, where n1, p2, and n2 μc-SiO$_x$:H layers are used, the total current of the solar cell is improved up to 27.8 mA/cm², as evident in Fig. 5. It shows that implementation of n1 and p2 μc-SiO$_x$:H layers results in the increase in the top cell current ($J_{QE,Top}$) by 0.8 mA/cm², while n2 μc-SiO$_x$:H layer is responsible for the improvement in ($J_{QE,Bot}$) at the wavelength range above 820 nm, consistent with reduced cell reflection in this wavelength range. We note that in the case of cell 5, a slight increase in cell reflection, *R* (see Fig. 5), is observed at the wavelengths between 450 and 620 nm and between 700 and 750 nm. A similar effect on reflection has been reported in ref. 10. Figure 5 indicates a gain in the total current of the tandem cell ($J_{QE,Sum}$) by 0.55 mA/cm² relative to the reference solar cell without μc-SiO$_x$:H layers. A part of the reduction in ($J_{QE,Bot}$) could be assigned to the increased cell reflection as noted earlier. This solar cell, prepared with n1, p2, and n2 μc-SiO$_x$:H layers shows a high initial efficiency of 13.1%, and 11.8% after 1000 h of light soaking. The *J*–*V* characteristics of this solar cell, measured with antireflection coating, in the initial and stabilized performance are summarized in Table 2.

Table 2. *J–V* characteristics: efficiency (η), fill factor (FF), open circuit voltage (V_{OC}), and short circuit current density (J_{SC}) of a tandem solar cell with μc-SiO_x:H layers in the initial and degraded (after 1000 h) conditions.

	η (%)	FF (%)	V_{OC} (V)	J_{SC} (mA/cm^2)
Initial	13.1	71.0	1.33	13.9
Stabilized	11.8	64.7	1.33	13.6

5. Conclusion

Electrical, optical, and structural properties of p- and n-type μc-SiO_x:H were investigated over a wide range of properties with respect to photovoltaic applications. We have found that at a given r_{CO2}, adding of PH_3 gas tends to increase crystallinity of the μc-SiO_x:H layers, while TMB tends to suppress crystalline growth. Our results demonstrate that the properties of doped μc-SiO_x:H can be conveniently adjusted to fulfil various requirements for applications in tandem solar cells. A remarkable increase in top cell current and overall efficiency because of incorporation of both p- and n-type μc-SiO_x:H layers demonstrate the suitability and high potential of μc-SiO_x:H as a functional layer in tandem devices. High efficiencies of 13.1% (initial) and 11.8% (stabilized) were achieved for tandem solar cells with doped μc-SiO_x:H layers.

Acknowledgement

The authors thank A. Bauer, R. Carius, M. Hülsbeck, J. Klomfaß, G. Schöpe, and C. Zahren for their contributions to this work. This work was partially supported by the German Federal Ministry for the Environment, Nature Conservation and Nuclear Safety (BMU) under contract No. 0325442D and by the EC under grant agreement No. 283501 (Fast Track).

References

1. D. Das, M. Jana, and A.K. Barua. Sol. Energy Mat. Sol. Cells, **63**, 285 (2000). doi:10.1016/S0927-0248(00)00035-0.
2. D. Domine, P. Buehlmann, J. Bailat, A. Billet, A. Feltrin, and C. Ballif. Phys. Stat. Sol. (RRL), **2**, 4, 163 (2008).
3. V. Smirnov, W. Böttler, A. Lambertz, H. Wang, R. Carius, and F. Finger. Phys. Status Solidi C, **7**, 1053 (2010).
4. P. Delli Veneri, L.V. Marcaldo, and I. Usatii. Appl. Phys. Lett. **97**(2), 023512 (2010).
5. A. Lambertz, T. Grundler, and F. Finger. J. Appl. Phys. **109**, 113109 (2011). doi:10.1063/1.3592208.
6. B. Yan, G. Yue, L. Sivec, J. Yang, S. Guha, and C.-S. Jiang. Appl. Phys. Lett. **99**, 113512 (2011). doi:10.1063/1.3638068.
7. V. Smirnov, A. Lambertz, B. Grootoonk, R. Carius, and F. Finger. J. Non-Cryst. Solids, **358**, 1954 (2012). doi:10.1016/j.jnoncrysol.2011.12.019.
8. A. Lambertz, F. Finger, B. Holländer, J.K. Rath, and R.E.I. Schropp. J. Non-Cryst. Solids, **358**, 1962 (2012). doi:10.1016/j.jnoncrysol.2011.12.047.
9. A. Lambertz, V. Smirnov, T. Merdzhanova, K. Ding, S. Haas, G. Jost, R.E.I. Schropp, F. Finger, and U. Rau. Sol. Energy Mat. Sol. Cells, **119**, 134 (2013). doi:10.1016/j.solmat.2013.05.053.
10. S. Kirner, O. Gabriel, B. Stannowski, B. Rech, and R. Schlatmann. Appl. Phys. Lett. **102**, 051906 (2013). doi:10.1063/1.4790279.
11. V. Smirnov, C. Das, T. Melle, A. Lambertz, M. Hülsbeck, R. Carius, and F. Finger. Mater. Sci. Eng. B, **159–160**, 44 (2009). doi:10.1016/j.mseb.2008.10.050.
12. IEC 60904-9 Photovolataic devices – Part 9: Solar simulator performance requirements. 2007.
13. A. Dasgupta, A. Lambertz, O. Vetterl, F. Finger, R. Carius, U. Zastrow, and H. Wagner. *In* Proceedings of the 16th European Photovoltaic Solar Energy Conference, Glasgow, UK, 1–5 May 2000. p. 557.
14. A. Matsuda, S. Yamasaki, K. Nakagawa, H. Okushi, K. Tanaka, S. Iizoma, M. Matsumura, and H. Yamamoto. Jpn. J. Appl. Phys. **19**, L305 (1980). doi:10.1143/JJAP.19.L305.